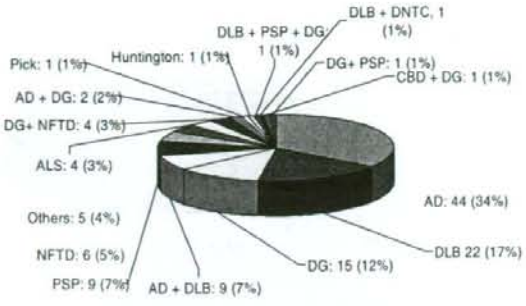

Fig. 2 Detailed degenerative pathology of with clinical dementia rating scale (CDR) 0.5 and CDR ≥ 1. (A) Degenerative pathology in CDR 0.5 consisted of 36% argyrophilic grain change (AGC), 31% Alzheimer change (AC), 24% the neurofibrillary tangle predominant change (NFTC) and 9% dementia with Lewy body disease change (DLBC). Those cases with combined degenerative pathology, for example, AC + DLBC, were counted twice to be included in both categories AC and DLBC. (B) Degenerative pathology in CDR ≥ 1 consisted of 43% Alzheimer's disease (AD), 26% dementia with Lewy bodies (DLB), 12% dementia with grain (DG) and 11% neurofibrillary tangle predominant form of dementia (NFTD). The higher frequency of AD and DLB among CDR ≥ 1, than that of AC and DLBC among CDR 0.5, could be best explained by faster speed of exacerbation in these two groups, in AGC and NFTC.

Table 1 Case profiles of CDR 0.5 with pure Alzheimer change

Age/ gender	Brain weight (g)	Stages of senile changes				ApoE genotyping
		NFT	SP	LB	AG	
82/F	1070	III	C	0	0	34
88/F	1030	III	C	0	0	34
88/M	1370	III	B	0	0	33
91/M	1155	III	C	0	0	34
94/F	1550	III	B	0	1	33
94/F	1080	III	B	0	2	33

SP, senile plaque; LB, Lewy body; AG, arygyrophilic grain; NFT, SP: Braak stage.[10] LB, AG: our stage.[6,7]

Senile tauopathy

We define "senile tauopathy" as tauopathy independent from Aβ accumulation, which includes argyrophilic grain disease (AGD), neurofibrillary tangle predominant disease (NFTD), progressive supranuclear palsy (PSP), corticobasal degeneration (CBD), diffuse neurofibrillary tangle disease with calcification (DNTC) and other unclassified tauopathy. PSP and CBD are classified into Parkinson's disease-related disorders, but in the aged cohort, their initial symptoms could be cognitive decline and these cases should instead be classified as senile tauopathy. Clinical characterization of AGD and NFTD is still underway, because they are often complicated with each other and also coexist with PSP or CBD.

Table 2 Case profiles of CDR 0.5 with pure argyrophilic grain disease (AGD)

Age/ gender	Brain weight (g)	Stages of senile changes				ApoE genotyping
		NFT	SP	LB	AG	
78	1150	II	A	1	3	34
80	1180	I	B	1	3	33
86	1177	II	B	1	3	33
93	1185	I	B	0	2	33
93	1190	II	A	0.5	2	33
94	1451	II	A	1	3	ND

SP, senile plaque; LB, Lewy body; AG, arygyrophilic grain; NFT, SP: Braak stage.[10] LB, AG: our stage.[6,7]

Table 3 Case profiles of CDR 0.5 with pure neurofibrillary tangle predominant change

Age/ gender	Brain weight (g)	Stages of senile changes				ApoE genotyping
		NFT	SP	LB	AG	
88/M	1130	III	A	0	0	33
89/F	1221	IV	0	0	0	34
91/M	1090	IV	0	1	1	33
93/F	1100	III	0	0	0	33
99/F	1200	III	A	0	0	33

SP, senile plaque; LB, Lewy body; AG, arygyrophilic grain; NFT, SP: Braak stage.[10] LB, AG: our stage.[6,7]

Table 4 Case profiles of CDR 0.5 with pure "dementia with Lewy body" change

Age/ gender	Brain weight (g)	Stages of senile changes				ApoE genotyping
		NFT	SP	LB	AG	
82/F†	973	I	0	2 (3‡)	0	33
88/M	1235	I	A	2 (3‡)	1	33
90/F	981	II	A	2 (5‡)	0	33

SP, senile plaque; LB, Lewy body; AG, arygyrophilic grain; NFT, SP: Braak stage.[10] LB, AG: our stage.[6,7]

†A history of delusion during her stay in the hospital. ‡Lewy body scores, defined by the first Consensus Guideline of Dementia with Lewy bodies.[9]

In this cohort, senile tauopathy was found among 57% of CDR0.5 cases and 33% of demented cases.

Case profiles of CDR 0.5 with single pathology

Alzheimer change in CDR 0.5

The case profiles are summarized in Table 1. The mean age was 89.5 years. All cases fulfilled the criteria of "early AD". The allelic frequency of apoE ε4 was 25%, which was higher than that in the total cases (10.1%).

Argyrophilic grain change in CDR 0.5

The case profiles are summarized in Table 2. The mean age was 87.3 years. Four of the six cases (67%) showed abundant AGs, fulfilling the criteria for dementia with grains.[7]

Table 5 Case profiles of CDR 0.5 with "hippocampal sclerosis"

Age/ gender	Brain weight (g)	Stages of senile changes				CVD lesion	Atherosclerosis
		NFT	SP	LB	AG		
94/F	850	II	0	0	1	–	Mild
89/M	1296	0	B	0	0	–	Mild

SP, senile plaque; LB, Lewy body; AG, arygyrophilic grain; CVD, cardiovascular disease; NFT, SP: Braak stage.[10] LB, AG: our stage.[6,7]

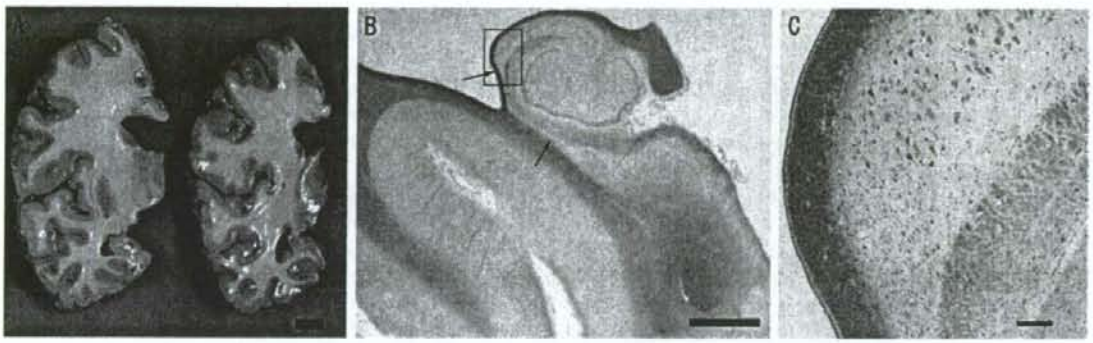

Fig. 3 Neuropathology of hippocampal sclerosis. (A) Macroscopic pathology of hippocampal sclerosis with serial unfixed coronal sections. Prominent atrophy of posterior hippocampus (bar = 1 cm). (B) Myelin-stained sections, demonstrating marked atrophy involving the CA1 and the subiculum (arrows). (Klüver-Barrera stain, bar = 0.5 cm). (C) Higher magnification of the hippocampus, indicated by a rectangle in section B, showing severe neuronal loss of CA1, relatively sparing CA2 (Klüver-Barrera stain, bar = 100 μm).

Neurofibrillary tangle predominant change in CDR 0.5

The case profiles are summarized in Table 3. The mean age of this group was highest (91.6 years).

Dementia with Lewy bodies – type change in CDR 0.5

The case profiles are summarized in Table 4. All cases showed amnesia as the chief complaint. All cases exhibited the presence of cortical Lewy bodies, fulfilling DLB limbic type.

Hippocampal sclerosis in CDR 0.5

The case profiles are summarized in Table 5. Both cases showed degeneration restricted to the anterior to posterior hippocampus (Fig. 3) without degenerative or vascular changes.

Neuropathologically unremarkable cases in CDR 0.5

The case profiles are summarized in Table 6. There was one case accompanied with severe compression myelopathy causing a bed-ridden state.

DISCUSSION

This study examined the pathological background of CDR 0.5 cases from serial autopsy cases from a general geriatric hospital, which roughly represent a general geriatric cohort. The results showed considerable differences from those obtained in memory clinics, where cases with AD represent the majority.

Table 6 Case profiles of CDR 0.5 without specific neuropathological changes

Age/ gender	Brain weight (g)	Stages of senile changes				ApoE genotyping
		NFT	SP	LB	AG	
76/F	1175	II	A	0	1	33
76/F	1280	I	A	0	0	33
79/M	1180	II	0	0	0	33
95/M	1032	II	B	0	0	34
97/F†	969	I	B	0	0	33

SP, senile plaque; LB, Lewy body; AG, arygyrophilic grain; NFT, SP: Braak stage.[10] LB, AG: our stage.[6,7]

†Bedridden state due to cervical compression myelopathy.

The pathological background of CDR 0.5 in our series consisted of AC, AGC, NFTC and DLBC, as well as vascular change and trauma. Special mention should be made of hippocampal sclerosis, which in Japan, has been neglected as secondary hypoxic/ischemic changes. Since these patients apparently survived the hypoxic/ischemic insults causing hippocampal sclerosis in recent advanced medical care, this pathology should be considered as a cause of cognitive decline, as stressed in the US.

A considerable number of cases showed non-specific pathology, making it difficult to explain the cognitive

decline. These cases may represent depression or reversible MCI. Many CDR 0.5 cases presented with various pathologies and it was difficult to determine which pathology most strongly contributed to cognitive decline with this type of retrospective study. Nevertheless, this study of cases with single neuropathological alterations definitely demonstrates that there were multiple pathological bases for CDR 0.5.

When the pathological background of CDR 0.5 was compared with that of dementia, they both shared each pathological component, but the incidences were different. The reason why the frequency of senile tauopathy was higher in CDR 0.5 than in CDR ≥1 was probably related to the speed in the progression of cognitive decline. In other words, AC/DLBC groups progress rapidly, while AGD/NFTC groups present with a more benign course, and thus the latter stay in CDR 0.5 longer. We are now examining cases of CDR 0.5 with MRI VSRAD, CSF biomarkers and PET scan, including fluorodeoxyglucose (FDG) and Pittsburgh Compound B (PIB). The results show that the cases presenting with normal Aβ 42 in the CSF and lacking cerebral cortical deposition of PIB show a slowly progressing course (data not shown).

From clinical longitudinal studies, MCI cases were classified into progressive, non-progressive and recovering subgroups. Our pathological study indicates that the first group may represent an AC/DLBC group, the second, an AGC/NFTC group and the last, unremarkable pathology.

Recently, neuropathological studies of mild cognitive impairment and cases of dementia followed from MCI stages were reported from the longitudinal prospective studies.[23,24] The results were similar to our findings, with highest frequency of AD, but definitely included cases of AGC/NFTC changes.

Our study confirmed that MCI or CDR 0.5 represents a stage of cognitive decline and can be explained by different pathological backgrounds. So MCI or CDR 0.5 should receive a diagnosis of early AD, DLB, DG, NFTD, VD or unremarkable pathology and the most appropriate method for intervention should be employed. For this purpose, we are now conducting multi-institutional prospective longitudinal studies.

REFERENCES

1. Hughes CP, Berg L, Danziger WL, Coben LA, Martin RL. A new clinical scale for the staging of dementia. *Br J Psychiatry* 1982; **140**: 566–572.
2. Petersen RC, Smith GE, Waring SC, Ivnik RJ, Tangalos EG, Kokmen E. Mild cognitive impairment: clinical characterization and outcome. *Arch Neurol* 1999; **56**: 303–308.
3. Folstein MF, Folstein SE, McHugh PR. "Mini-mental state". A practical method for grading the cognitive state of patients for the clinician. *J Psychiatr Res* 1975; **12**: 189–198.
4. Hasegawa K, Inoue K, Moriya K. An investigation of dementia rating scale for the elderly. *Seishin Igaku* 1974; **16**: 965–969.
5. Katoh S, Simogaki H, Onodera A *et al.* Development of the revised version of Hasegawa's dementia scale (HDS-R). *Ronen Seisin Igaku Zassi* 1991; **2**: 1339–1347.
6. Saito Y, Ruberu NN, Sawabe M *et al.* Lewy body-related alpha-synucleinopathy in aging. *J Neuropathol Exp Neurol* 2004; **63**: 742–749.
7. Saito Y, Ruberu NN, Sawabe M *et al.* Staging of argyrophilic grains: an age-associated tauopathy. *J Neuropathol Exp Neurol* 2004; **63**: 911–918.
8. Mirra SS, Heyman A, McKeel D *et al.* The Consortium to Establish a Registry for Alzheimer's Disease (CERAD). Part II. Standardization of the neuropathologic assessment of Alzheimer's disease. *Neurology* 1991; **41**: 479–486.
9. McKeith IG, Galasko D, Kosaka K *et al.* Consensus guidelines for the clinical and pathologic diagnosis of dementia with Lewy bodies (DLB): report of the consortium on DLB international workshop. *Neurology* 1996; **47**: 1113–1124.
10. Braak H, Braak E. Neuropathological stageing of Alzheimer-related changes. *Acta Neuropathol (Berl)* 1991; **82**: 239–259.
11. Hauw JJ, Daniel SE, Dickson D *et al.* Preliminary NINDS neuropathologic criteria for Steele–Richardson–Olszewski syndrome (progressive supranuclear palsy). *Neurology* 1994; **44**: 2015–2019.
12. Yamaguchi H, Haga C, Hirai S, Nakazato Y, Kosaka K. Distinctive, rapid, and easy labeling of diffuse plaques in the Alzheimer brains by a new methenamine silver stain. *Acta Neuropathol (Berl)* 1990; **79**: 569–572.
13. Gallyas F. Silver staining of Alzheimer's neurofibrillary changes by means of physical development. *Acta Morphol Acad Sci Hung* 1971; **19**: 1–8.
14. Fujiwara H, Hasegawa M, Dohmae N *et al.* alpha-Synuclein is phosphorylated in synucleinopathy lesions. *Nat Cell Biol* 2002; **4**: 160–164.
15. Saito Y, Kawashima A, Ruberu NN *et al.* Accumulation of phosphorylated alpha-synuclein in aging human brain. *J Neuropathol Exp Neurol* 2003; **62**: 644–654.
16. Hatsuta H, Saito Y, Ikemura M *et al.* Extension staging criteria of cerebral amyloid angiopathy. *Neuropathology* 2006; **26**: A9.
17. Murayama S, Saito Y. Neuropathological diagnostic criteria for Alzheimer's disease. *Neuropathology* 2004; **24**: 254–260.

18. The National Institute on Aging, and Reagan Institute Working Group on Diagnostic Criteria for the Neuropathological Assessment of Alzheimer's Disease. Consensus recommendations for the postmortem diagnosis of Alzheimer's disease. *Neurobiol Aging* 1997; **18** (4 Suppl): S1–S2.
19. Jellinger KA. Dementia with grains (argyrophilic grain disease). *Brain Pathol* 1998; **8**: 377–386.
20. Jellinger KA, Bancher C. Senile dementia with tangles (tangle predominant form of senile dementia). *Brain Pathol* 1998; **8**: 367–376.
21. Roman GC, Tatemichi TK, Erkinjuntti T *et al.* Vascular dementia: diagnostic criteria for research studies. Report of the NINDS-AIREN International Workshop. *Neurology* 1993; **43**: 250–260.
22. Saito Y, Nakahara K, Yamanouchi H, Murayama S. Severe involvement of ambient gyrus in dementia with grains. *J Neuropathol Exp Neurol* 2002; **61**: 789–796.
23. Jicha GA, Parisi JE, Dickson DW *et al.* Neuropathologic outcome of mild cognitive impairment following progression to clinical dementia. *Arch Neurol* 2006; **63**: 674–681.
24. Petersen RC, Parisi JE, Dickson DW *et al.* Neuropathologic features of amnestic mild cognitive impairment. *Arch Neurol* 2006; **63**: 665–672.

Journal of Neuroscience Research 85:3098–3108 (2007)

Molecular Chaperone-Mediated Tau Protein Metabolism Counteracts the Formation of Granular Tau Oligomers in Human Brain

N. Sahara,[1]* S. Maeda,[1] Y. Yoshiike,[1] T. Mizoroki,[1] S. Yamashita,[1] M. Murayama,[1] J.-M. Park,[1] Y. Saito,[2,3] S. Murayama,[2] and A. Takashima[1]

[1]Laboratory for Alzheimer's Disease, RIKEN Brain Science Institute, Wako-shi, Saitama, Japan
[2]Department of Neuropathology, Tokyo Metropolitan Institute of Gerontology, Tokyo, Japan
[3]Department of Pathology, Tokyo Metropolitan Geriatric Hospital, Tokyo, Japan

Intracellular accumulation of filamentous tau proteins is a defining feature of neurodegenerative diseases termed *tauopathies*. The pathogenesis of tauopathies remains largely unknown. Molecular chaperones such as heat shock proteins (HSPs), however, have been implicated in tauopathies as well as in other neurodegenerative diseases characterized by the accumulation of insoluble protein aggregates. To search for in vivo evidence of chaperone-related tau protein metabolism, we analyzed human brains with varying degrees of neurofibrillary tangle (NFT) pathology, as defined by Braak NFT staging. Quantitative analysis of soluble protein levels revealed significant positive correlations between tau and Hsp90, Hsp40, Hsp27, α-crystallin, and CHIP. An inverse correlation was observed between the levels of HSPs in each specimen and the levels of granular tau oligomers, the latter of which were isolated from brain as intermediates of tau filaments. We speculate that HSPs function as regulators of soluble tau protein levels, and, once the capacity of this chaperone system is saturated, granular tau oligomers form virtually unabated. This is expressed pathologically as an early sign of NFT formation. The molecular basis of chaperone-mediated protection against neurodegeneration might lead to the development of therapeutics for tauopathies.

Key words: tau; oligomer; heat shock protein; molecular chaperone; Braak stage

Intracellular accumulation of filamentous tau proteins is a defining feature of neurodegenerative diseases, including Alzheimer's disease (AD), progressive supranuclear palsy, corticobasal degeneration, Pick's disease, and frontotemporal dementia with Parkinsonism linked to chromosome 17, all known collectively as *tauopathies* (Lee et al., 2001). Tau is a highly soluble and natively unfolded protein dominated by a random coil structure in solution (Schweers et al., 1995). It is believed that aberrant modifications of tau, including phosphorylation, truncation, and conformational changes, induce filamentous aggregation (Alonso et al., 1996; Gamblin et al., 2003; Garcia-Sierra et al., 2003). In AD and related tauopathies correlated with dementia, tau generates insoluble aggregates (Arriagada et al., 1992). Although the mechanism underlying the conversion of tau protein from a soluble state to one of insoluble aggregates remains unclear, molecular chaperones such as heat shock proteins (HSPs) have been implicated in these tauopathies (Dabir et al., 2004; Nemes et al., 2004).

Molecular chaperones have essential roles in many cellular processes, including protein folding, targeting, transport, degradation, and signal transduction (Hartl and Hayer-Hartl, 2002). In addition to molecular chaperones, cells have evolved two mechanisms for degrading misfolded proteins, the ubiquitin-proteasome pathway and lysosome-mediated autophagy. The collective activities of molecular chaperones, the ubiquitin-proteasome system, and lysosome-mediated autophagy are normally sufficient to prevent the accumulation of misfolded proteins. In AD, Parkinson's disease, familial amyotrophic lateral sclerosis, and polyglutamine diseases, plaques and/or inclusion bodies that characterize these diseases colocalize with various molecular chaperones (Muchowski and Wacker, 2005) and components of the ubiquitin-proteasome degradation system (Sherman and Goldberg, 2001).

Recently, the carboxyl terminus of Hsc70-interacting protein (CHIP) was demonstrated to regulate tau

Contract grant sponsor: RIKEN BSI; Contract grant sponsor: Grant-in-Aid for Science Research from the Japanese Ministry of Education, Science, Sports and Culture (to A.T.).

*Correspondence to: N. Sahara, Laboratory for Alzheimer's Disease, RIKEN Brain Science Institute, Wako-shi, Saitama 351-0198, Japan. E-mail: saharanaruhiko@brain.riken.jp

Received 28 February 2007; Revised 25 April 2007; Accepted 26 April 2007

Published online 12 July 2007 in Wiley InterScience (www.interscience.wiley.com). DOI: 10.1002/jnr.21417

ubiquitination and degradation (Hatakeyama et al., 2004; Petrucelli et al., 2004; Shimura et al., 2004b). CHIP is a key molecule in protein quality control processes that link the ubiquitin-proteasome and chaperone systems. We previously found increased levels of CHIP in AD brains that were inversely proportional to the amount of accumulated tau (Sahara et al., 2005). Deletion of CHIP in mice, however, failed to promote tau aggregation (Sahara et al., 2005; Dickey et al., 2006b). Thus, these observations could not clarify the precise roles of the chaperone and ubiquitin-proteasome systems in the pathogenesis of tauopathies. Immunohistochemical studies also showed that AD brains contain very few accumulations of CHIP within neurofibrillary tangle (NFT)-bearing neuron (Petrucelli et al., 2004). Indeed, the colocalization of tau pathology and chaperones varies, as demonstrated by immunostaining for tau, Hsp27, αB-crystallin (Dabir et al., 2004), Hsp70, and Hsp90 (Dou et al., 2003). These observations suggest that tau in a misfolded conformation or state, not tau in an irreversible filamentous state, may exist and be directly regulated as a chaperone client. For this reason, we continue to search for intermediate forms of tau fibrils by examining assembled recombinant tau and tau in human brain extracts. Atomic force microscopy (AFM) has revealed a granular-shaped prefilamentous form of tau in both in vitro and in vivo preparations (Maeda et al., 2006, 2007).

In the present study, human brains with varying degrees of Braak-staged NFT pathology were analyzed to assess tau protein quality control in vivo. Biochemically, HSPs and related proteins were quantitatively analyzed to examine the relationship between tau and HSPs. A positive correlation was revealed between tau and certain HSPs in terms of soluble protein levels. Moreover, we discovered an inverse correlation between the levels of granular tau oligomer and those of HSPs. These findings suggest that molecular chaperones interact with soluble tau protein to down-regulate the formation of granular tau oligomer.

MATERIALS AND METHODS

Post-Mortem Brains

Brain tissue was obtained from the Brain Bank for Aging Research at Tokyo Metropolitan Institute of Gerontology (TMIG) and Tokyo Metropolitan Geriatric Hospital (TMGH). Frontal and temporal cortices were examined from each brain specimen. Senile plaques and NFTs were classified based on quantitative pathological features according to Braak criteria (Braak and Braak, 1991). Demographic information for all brain specimens analyzed is presented in Table I and in a previous report (Maeda et al., 2006). This study was approved by the Institutional Review Board (IRB) of TMIG and TMGH as well as the RIKEN IRB.

Tissue Extraction

Frontal and temporal cortices from each subject were homogenized separately in three volumes of Tris-buffered saline (TBS) containing protease and phosphatase inhibitors [25 mM Tris/HCl, pH 7.4; 150 mM NaCl; 1 mM EDTA; 1 mM EGTA; 5 mM sodium pyrophosphate; 30 mM β-glycerophosphate; 30 mM sodium fluoride; and 1 mM phenylmethylsulfonyl fluoride (PMSF)]. The homogenates were centrifuged at 27,000*g* for 15 min at 4°C to obtain supernatant (TBS sup) and pellet fractions. Pellets were rehomogenized in three volumes of high-salt/sucrose buffer (0.8 M NaCl; 10% sucrose; 10 mM Tris/HCl, pH 7.4; 1 mM EGTA; 1 mM PMSF) and centrifuged as described above. The supernatants were collected and incubated with sarkosyl (Sigma, St. Louis, MO; 1% final concentration) for 1 hr at 37°C, followed by centrifugation at 150,000*g* for 1 hr at 4°C to obtain salt and sarkosyl-soluble and sarkosyl-insoluble pellets (srk-ppt fractions).

TABLE I. Demographic and Neuropathological Characteristics of Subjects*

Case no.	Age (years)	Sex	PMI (hr:min)	Braak stage[a] NFT	Braak stage[a] SP	Insoluble tau[b] Frontal	Insoluble tau[b] Temporal
1	52	M	15:51	0	0	0.86	0.70
2	69	F	11:48	0	A	0.45	1.06
3	82	F	39:04	0	0	2.34	1.23
4	87	M	70:10	0	0	0	1.86
5	78	M	2:02	0	0	0	9.73
6	66	F	9:51	0	B	0	2.44
7	81	M	3:00	I	B	1.00	10.82
8	97	F	2:40	I	B	7.00	3.34
9	84	M	47:25	I	B	0	4.48
10	87	M	4:25	I	C	1.94	19.1
11	93	M	20:49	I	C	3.38	69.5
12	86	F	6:50	III	C	1.93	100.4
13	94	M	13:00	III	C	2.56	73.3
14	87	F	4:21	III	C	6.81	209.5
15	82	F	10:32	III	C	31.1	184.8
16	89	F	16:11	III	C	7.03	88.6
17	90	F	64:07	V	C	182.5	2189.6
18	86	F	19:51	V	C	86.2	1026.5
19	93	F	13:28	V	C	169.8	1091.2
20	70	M	35:42	V	C	582.8	1580.1
21	80	F	6:41	V	C	9.60	223.4

*NFT, neurofibrillary tangle; SP, senile plaque; PMI, post-mortem interval.

[a]For the staging of NFTs and SPs, Braak and Braak criteria were applied (Braak and Braak, 1991).

[b]The relative score of sarkosyl-insoluble tau was measured by quantifying PHF1 immunoreactivity.

Western Blotting

Fractionated tissue extracts were dissolved in sample buffer containing β-mercaptoethanol (0.01%). The boiled extracts were separated by gel electrophoresis on 10% or 4–20% gradient SDS-PAGE gels and transferred onto nitrocellulose membranes (Schleicher & Schuell Bioscience, Dassel, Germany). After blocking with a solution of 5% nonfat milk and 0.1% Tween-20 in PBS, the membranes were incubated with various antibodies, washed to remove excess antibodies, and then incubated with peroxidase-conjugated goat anti-

rabbit IgG (1:5,000; Jackson Immunoresearch, West Grove, PA) or anti-mouse IgG (1:5,000; Jackson Immunoresearch). Bound antibodies were detected by using an enhanced chemiluminescence system, SuperSignal West Pico (Pierce Biotechnology, Rockford, IL). Quantitation and visual analysis of immunoreactivity were performed with a computer-linked LAS-3000 Bio-Imaging Analyzer System (Fujifilm, Tokyo, Japan) in the software Image Gauge 3.0 (Fujifilm).

Antibodies

Polyclonal antibody E1, which is specific for human tau (aa 19–33; Sahara et al., 2005), and polyclonal antibody tauC, which is specific for the C-terminus of tau (aa 422–438; Sato et al., 2002), were produced in our laboratory. Monoclonal antibody Tau5, which is against an epitope located within the middle region of tau, was purchased from Biosource International (Camarillo, CA). PHF1, which is specific for tau phosphorylated at Ser396/Ser404, was provided by Dr. Peter Davies (Jicha et al., 1999). Polyclonal CHIP antibodies (R1) were produced in rabbits (Imai et al., 2002). Monoclonal antibodies to Hsp90 (Santa Cruz Biotechnology, Santa Cruz, CA), Hsp70 (Chemicon, Temecula, CA), Hsp60 (Stressgen, San Diego, CA), Hsp27 (Stressgen), αB-crystallin (Stressgen), β-tubulin (Sigma), β-actin (Sigma), glyceraldehyde-3-phosphate dehydrogenase (GAPDH; Chemicon), and neuron-specific enolase (NSE; Upstate, Charlottesville, VA) were purchased. Polyclonal antibodies against Hsc70 and Hsp40 were purchased from MBL and Stressgen. For Western blotting, antibodies were used at the following dilutions in blocking solution: E1, 1:5,000; tau5, 1:2,000; tauC, 1:5,000; PHF1, 1:2,000; CHIP, 1:5,000; Hsp90, 1:2,000; Hsp70, 1:1,000; Hsc70, 1:1,000; Hsp60, 1:5,000; Hsp40, 1:10,000; Hsp27, 1:1,000; αB-crystallin, 1:1,000; Akt, 1:2,000; β-tubulin, 1:5,000; β-actin, 1:10,000; GAPDH, 1:5,000; NSE, 1:1,000.

Coimmunoprecipitation Analysis

TBS-soluble fractions were incubated with anti-tau antibody JM (an antibody against the longest isoform of recombinant human tau; Takashima et al., 1998) for 2 hr at 4°C. Protein G-sepharose (GE Healthcare Bioscience, Piscataway, NJ) equilibrated in TBS was added to the mixture, which was then rotated overnight at 4°C. The resin was separated by centrifugation, washed four times with TBS, and then boiled in SDS sample buffer. Samples were subjected to SDS-PAGE, with subsequent immunoblotting with antibodies against Hsp90, Hsp70, β-tubulin, tau (anti-tau antibody HT7; Innogenetics, Zwijndrecht, Belgium), and NSE.

Purification of Granular Tau Oligomers

Enriched granular tau oligomer preparations were prepared as previously described (Maeda et al., 2006, 2007). Briefly, soluble fractions of human brain extracts (starting wet weight was ~12 g) were loaded onto an immunoaffinity column containing anti-tau antibody-conjugated Sepharose. Eluted samples were further purified by sucrose-step gradient centrifugation. Granular tau oligomer-enriched fractions were morphologically characterized by AFM.

Atomic Force Microscopy

Samples were dropped onto freshly cleaved mica and left in place for 30 min prior to AFM assessment. After washing the mica with water, we examined the tau-containing samples in solution using a Nanoscope IIIa (Digital Instruments, Santa Barbara, CA) set to tapping mode. OMCL-TR400PSA (Olympus, Tokyo, Japan) was used as a cantilever. The resonant frequency was about 9 kHz. We examined four different areas (4 μm^2) of the mica surface covered with granular aggregates. These areas were analyzed with NIH Image 1.63 (developed at The National Institute of Mental Health and available on the Internet at http://rsb.info.nih.gov/nih-image/), and summations of four different areas were demonstrated.

Incubation of Recombinant Tau and Fluorescence Spectroscopy

Recombinant human tau (2N4R) was expressed in *Escherichia coli* BL21(DE3) and partially purified as described previously (Hasegawa et al., 1998). The degree of tau aggregation was determined using thioflavin T (ThT). The tau stock solution was diluted to 10 μM in a solution containing PBS (pH 7.4) and 10 μM ThT (Aldrich Chemical, Milwaukee, WI), then loaded into 96-well Black Cliniplates (Thermo Labsystems, Yokohama, Japan). Tau assembly was initiated by adding 10 μM heparin (Acros Organics, Geel, Belgium) and incubating mixtures (final volume of 50 μl per well) at 37°C. To analyze the effects of HSPs, 0.1 μM or 1 μM Hsp70 (Sigma) and 0.1 μM or 1 μM Hsp40 proteins (Stressgen) were added alone or in combination to the aggregation reaction in the presence of 1 mM ATP at time zero. Fluorescence was measured with an ARVO MX Multilabel counter (PerkinElmer, Waltham, MA) at an excitation wavelength of 440 nm and an emission wavelength of 486 nm. Measurements were carried out at the time points indicated.

Fig. 1. Immunoblotting of sarkosyl-insoluble and TBS-soluble tau in frontal and temporal cortices from aged human brains. **A:** Western blots of sarkosyl-insoluble fractions in human frontal and temporal cortices. Samples were categorized as Braak NFT stage 0 (lanes 1–6), stage I (lanes 7–11), stage III (lanes 12–16), and stage V (lanes 17–21). Samples derived from brains (2–20 mg wet weight) were separated by SDS-PAGE, blotted, then probed with PHF1 antibody. Blot of frontal cortical samples was obtained from longer exposure time than that of temporal cortical samples. **B:** Western blots of TBS-soluble tau in human frontal and temporal cortices. Equal volumes of TBS-soluble fraction derived from 0.33 mg wet weight of brain were separated by SDS-PAGE, blotted, then probed with E1 (specific for N-terminus region of tau), tau5 (specific for the middle region), and tauC (specific for C-terminus region) antibodies. **C:** Western blots of TBS-soluble tau in human frontal and temporal cortices. Equal volumes of TBS-soluble fraction were separated by SDS-PAGE, blotted, then probed with the indicated panel of antibodies.

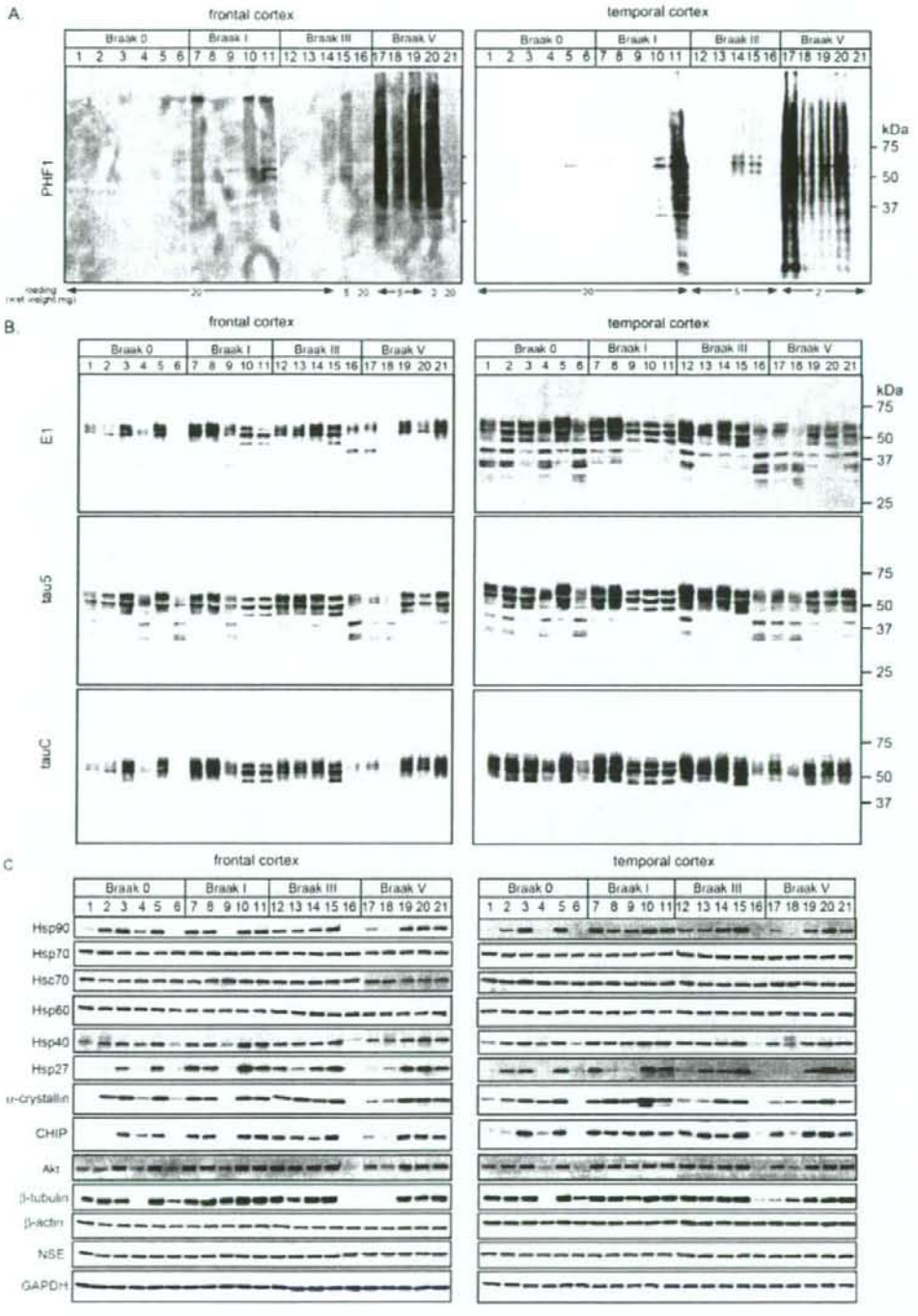
A.
frontal cortex
temporal cortex
Braak 0
Braak I
Braak III
Braak V
1 2 3 4 5 6 7 8 9 10 11 12 13 14 15 16 17 18 19 20 21
PHF1
kDa
75
50
37
B.
E1
tau5
tauC
25
C
Hsp90
Hsp70
Hsc70
Hsp60
Hsp40
Hsp27
α-crystallin
CHIP
Akt
β-tubulin
β-actin
NSE
GAPDH

Figure 1.

Statistical Analysis

The statistical significance between groups was assessed by the Mann-Whitney test. The correlation between the level of tau and other proteins was tested using Spearman correlation. Data were analyzed with Prism for Macintosh version 4.0b (Graphpad, San Diego, CA), and significance levels were set at $P < 0.05$.

RESULTS

Sarkosyl-Insoluble Tau in Human Brain

The neuropathological diagnoses of 21 cases were determined by using criteria for degenerative dementia as previously reported (Saito et al., 2002). To verify NFT pathology, we performed Western blotting on sarkosyl-insoluble fractions obtained from these 21 cases. The amounts of sarkosyl-insoluble tau in both frontal and temporal cortices correlated well with various Braak NFT stages (Fig. 1A, Table I). Immunoblots of fractions from Braak V-staged brains displayed the typical triplet bands and smear patterns of PHF1-positive tau. Although low sarkosyl-insoluble tau levels correlated well with Braak 0 and I stages—stages seen during normal brain aging characterized by the absence of NFT pathology in frontal and temporal cortices—weak PHF1-positive tau immunostaining was observed in one Braak 0 brain (case 5) and three Braak I brains (cases 7, 10, and 11; Fig. 1A, Table I). Indeed, some discrepancies have been reported regarding insoluble tau levels and NFT scores of brains staged at Braak stages I–III (Katsuno et al., 2005). Together, these results indicated that the biochemical analysis was more sensitive in detecting precursors of NFTs (i.e., PHF1-positive tau) than was the Braak neuropathological classification method. Nonetheless, for one Braak V brain (case 21), we detected very low levels of sarkosyl-insoluble tau. In case 21, these levels were equivalent to those detected in Braak III brains (Table I), suggesting that, despite reliable neuropathological diagnosis, an unknown tau modification might have occurred in this case. In any case, it is important to identify an early biochemical indicator of AD rather than to measure levels of sarkosyl-insoluble tau.

TBS-Soluble Tau Protein Profiles in Human Brains

As shown in Figure 1B, a wide range of TBS-soluble tau levels and variable Western blot profiles were observed among the human brains that we analyzed. Although we suspected that protein degraded during post-mortem intervals, the amounts of TBS-soluble tau in frontal and temporal cortices did not correlate with different postmortem intervals (Fig. 2A,B). For most of the samples, E1 and tau5 antibodies, which recognize the amino terminus and the middle regions of tau, respectively, immunostained low-molecular-weight bands ranging from 30 to 40 kDa (Fig. 1B). These bands, however, were not detectable with tauC antibody, which recognizes the carboxyl terminus of tau. This suggests that carboxyl-terminal-truncated tau fragments 30–40 kDa in size were present in these samples. For each case, the profile of tau protein in frontal cortex and that in temporal cortex appeared quite similar (Fig. 1B). Moreover, the relative levels of tau protein in frontal and temporal cortices were closely correlated ($P < 0.001$, Spearman correlation analysis). This result indicated that tau protein modification was conserved in different brain regions. Comparison of the amounts of TBS-soluble tau in brains of different Braak stages revealed significant differences in the frontal and temporal cortices of Braak I and V brains (Fig. 2G,H). These differences might be due to a conversion in tau protein solubility that results from excessive posttranslational modifications in Braak V brains, leading to the formation of filamentous insoluble tau. However, we did not observe a significant inverse correlation between TBS-soluble tau and sarkosyl-insoluble tau levels. Further study will be needed to clarify why Braak I and V brains contain different levels of soluble tau protein.

Correlation Between Tau Protein and HSPs

We used a panel of antibodies to identify HSPs (Hsp90, Hsp70, Hsc70, Hsp60, Hsp40, Hsp27, α-crystallin) and cochaperone CHIP in human frontal and temporal cortices (Fig. 1C). As with TBS-soluble tau levels, Hsp90 and NSE protein levels in frontal and temporal cortices did not correlate with different post-mortem intervals (Fig. 2C–F). Quantitative analysis of soluble protein levels in frontal cortices revealed significant positive correlations between tau and some HSPs (Hsp90, Hsp40, Hsp27, α-crystallin), CHIP, Akt, and β-tubulin (Table II). We obtained comparable results for soluble protein levels in temporal cortices (Fig. 1, Table II). Hsp90, Hsp40, Hsp27, α-crystallin, CHIP, Akt, and β-tubulin levels varied across different Braak stages, with

Fig. 2. Effect of post-mortem time and Braak NFT stage on relative protein levels. **A–F:** Relationship between postmortem interval (hours) and soluble protein levels. The relative amount of TBS-soluble tau in frontal (A) and temporal (B) cortices was calculated by dividing the intensity of tauC-immunoreactive bands by the intensity of GAPDH-positive bands. The relative amounts of Hsp90 in frontal (C) and temporal (D) cortices and NSE in frontal (E) and temporal (F) cortices were calculated by dividing the appropriate band intensity by the band intensity of GAPDH. The relative amount of protein in case 7 was always normalized to 1. **G,H:** The relative levels of TBS-soluble tau in frontal (G) and temporal (H) cortices were compared for each Braak NFT stage. The relative amounts of TBS-soluble tau, as shown in A and B, were categorized accordingly into Braak NFT stage 0, I, III, or V. The results are shown as scatterplots of mean values. $^{*}P < 0.05$, $^{**}P < 0.01$.

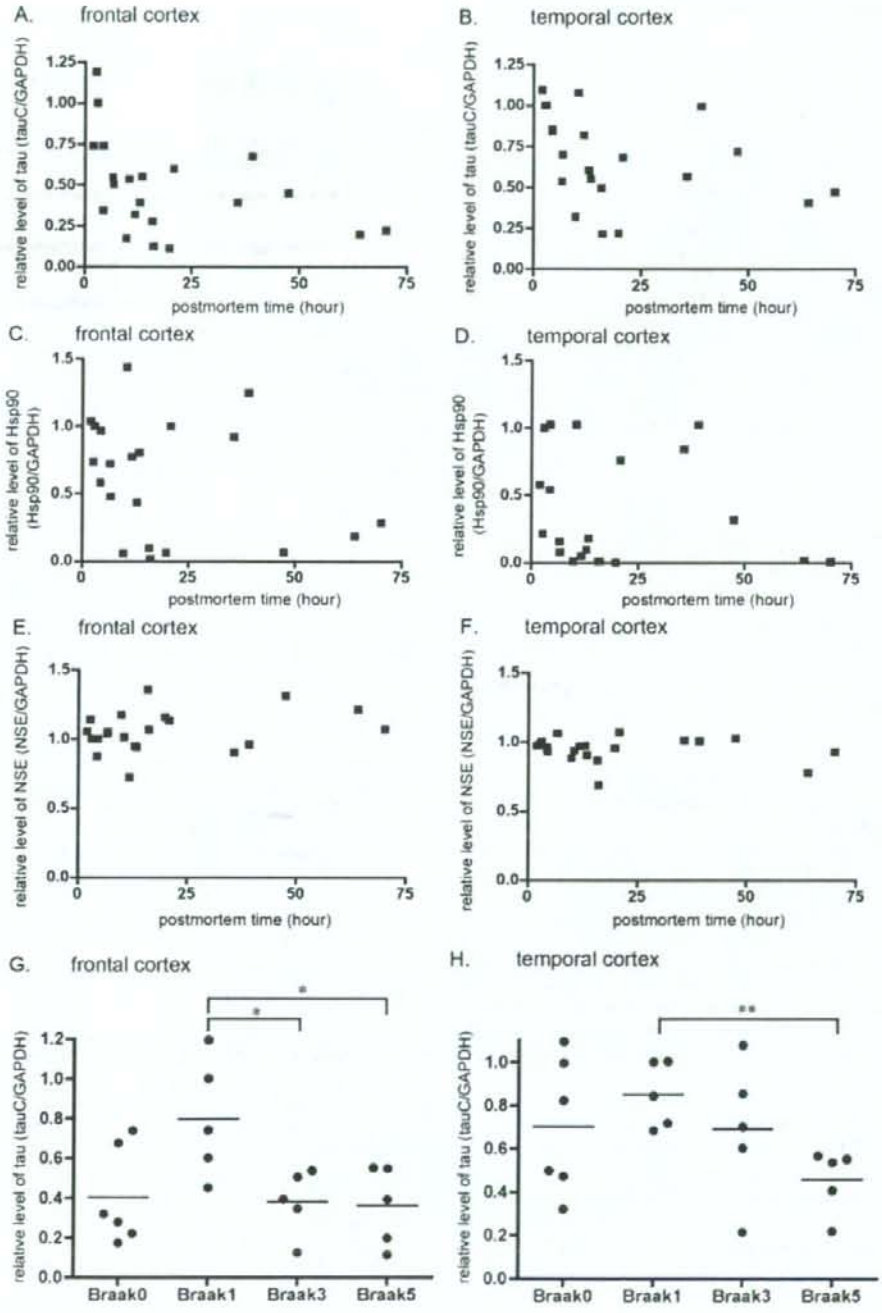
A.
frontal cortex
relative level of tau (tauC/GAPDH)
postmortem time (hour)
B.
temporal cortex
relative level of tau (tauC/GAPDH)
postmortem time (hour)
C.
frontal cortex
relative level of Hsp90 (Hsp90/GAPDH)
postmortem time (hour)
D.
temporal cortex
relative level of Hsp90 (Hsp90/GAPDH)
postmortem time (hour)
E.
frontal cortex
relative level of NSE (NSE/GAPDH)
postmortem time (hour)
F.
temporal cortex
relative level of NSE (NSE/GAPDH)
postmortem time (hour)
G.
frontal cortex
relative level of tau (tauC/GAPDH)
Braak0
Braak1
Braak3
Braak5
H.
temporal cortex
relative level of tau (tauC/GAPDH)
Braak0
Braak1
Braak3
Braak5

Figure 2.

TABLE II. Regional Correlation Analysis Between Tau and Other Proteins*

	Frontal cortex		Temporal cortex	
	Spearman regression	*P* value	Spearman regression	*P* value
Hsp90	0.789	<0.001	0.794	<0.001
Hsp70	−0.242	0.291	−0.186	0.420
Hsc70	−0.190	0.410	−0.143	0.537
Hsp60	0.085	0.714	−0.251	0.273
Hsp40	0.828	<0.001	0.723	<0.001
Hsp27	0.757	<0.001	0.562	0.008
α-Crystallin	0.801	<0.001	0.707	<0.001
CHIP	0.739	<0.001	0.751	<0.001
Akt	0.869	<0.001	0.768	<0.001
β-Tubulin	0.833	<0.001	0.779	<0.001
β-Actin	0.400	0.072	0.197	0.391
NSE	−0.283	0.214	0.449	0.041

*Soluble tau levels were obtained by dividing the intensity of tauC-immunopositive bands by the intensity of GAPDH-positive bands.

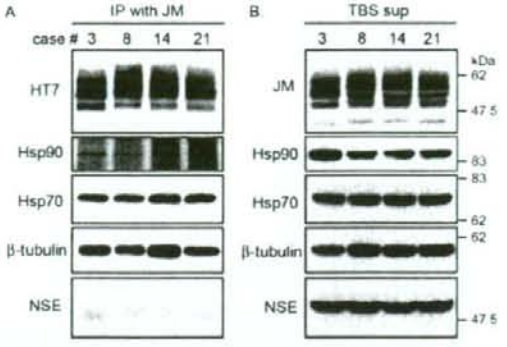

Fig. 3. Coimmunoprecipitation assay of human brain extracts. **A:** TBS-soluble fractions derived from temporal cortices (cases 3, 8, 14, and 21) were immunoprecipitated with anti-tau antibody JM. The resulting samples were immunoblotted with antibodies against HT7, Hsp90, Hsp70, β-tubulin, and NSE. **B:** TBS-soluble fractions were also subjected to SDS-PAGE and immunoblotted with the indicated antibodies.

samples from Braak I-staged brains tending to contain more of these proteins. In contrast, Hsp70, Hsc70, Hsp60, β-actin, NSE, and GAPDH levels remained steady across different Braak stages and within each cortical region. Quantitative analysis clearly showed that the levels of all soluble proteins did not correlate with the levels of sarkosyl-insoluble tau, more of which was recovered in temporal cortices than in frontal cortices. Moreover, we did not observe any significant correlation between HSP levels and senile-plaque stage (Table I). These data suggest that a molecular chaperone complex (Hsp90, Hsp40, Hsp27, α-crystallin, and CHIP) interacts with Akt, β-tubulin, and tau as client proteins in aged human brains and that this complex is elevated during the Braak I stage.

To determine whether tau and the chaperone proteins physiologically interact in human brain, we analyzed brain extracts using a coimmunoprecipitation assay. Regardless of Braak stage, tau coimmunoprecipitated with Hsp90, Hsp70, and β-tubulin but with not NSE (Fig. 3). Surprisingly, Hsp70 was more efficiently recovered by anti-tau immunoprecipitation than Hsp90. Although the direct interaction between tau and these HSPs remains to be demonstrated, these data support the hypothesis that tau and Hsp90/Hsp70 physiologically interact.

Correlation Between HSP Levels in Soluble Fraction and Granular Tau Oligomer

Previously, the identification of granular tau oligomers as intermediates of tau filaments from human frontal cortices was reported (Maeda et al., 2006). Granular tau oligomer levels in frontal cortex were increased even in brains displaying Braak I characteristics (Fig. 4A,B), suggesting that granular tau oligomers may form before NFTs form. To evaluate these oligomers further, we compared oligomer levels from each specimen to HSP levels and observed a significant inverse correlation between oligomer and Hsp90 levels (Fig. 4D; oligomers vs. Hsp90, $P = 0.045$) and between oligomer and α-crystallin levels (oligomers vs. α-crystallin, $P = 0.029$). When data from Braak 0 samples were excluded from the correlation analyses, we found that Hsp40, Hsp27, α-crystallin, CHIP, and Akt levels also showed a significant inverse correlation with oligomer levels (Hsp40 $P < 0.001$, Hsp27 $P < 0.001$, α-crystallin $P < 0.001$, CHIP $P = 0.0015$, Akt $P = 0.0033$). Because the levels of these HSPs positively correlate with the levels of TBS-soluble tau, we were able to determine the relationship between tau oligomers and TBS-soluble tau in Braak-staged aged brains. Indeed, oligomer levels inversely correlated with TBS-soluble tau levels (Fig. 4C; oligomers vs. tauC-positive tau, $P = 0.015$). These findings suggest that TBS-soluble tau is a target of the HSP-mediated refolding complex, whereas granular tau oligomers are counterparts of this complex.

HSPs Prevent In Vitro Tau Self-Aggregation

To study the biochemical interaction between tau protein and HSPs, we analyzed in vitro tau polymerization in the presence and absence of Hsp40 and/or Hsp70 by using a ThT-binding assay. The thioflavin assay is the most commonly used assay to assess real-time tau assembly, because ThT binds β-sheet structures. With increased binding, more intense fluorescent signals are emitted (Kuret et al., 2005). As we previously described (Maeda et al., 2007), tau self-assembly was induced by adding heparin, after which ThT fluorescence levels plateaued after 100 hr (Fig. 5A). Tau prepared in the absence of heparin displayed no measurable

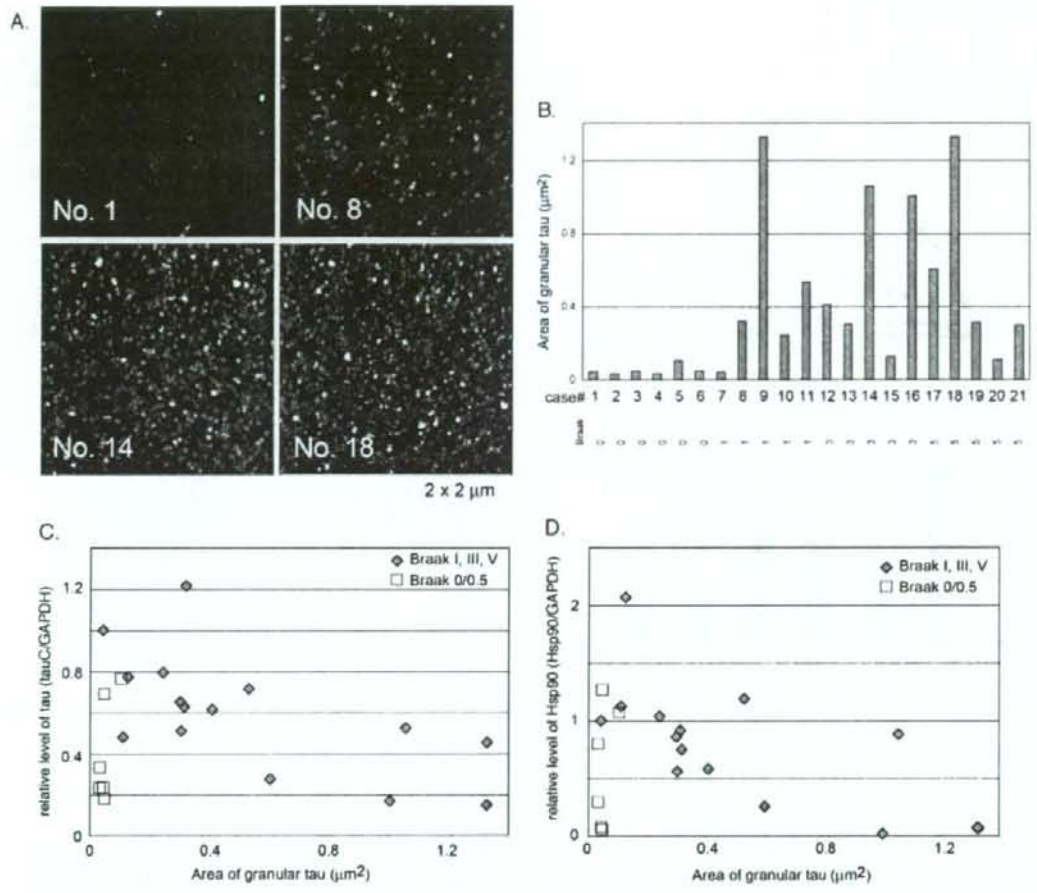

Fig. 4. Quantitative analysis of granular tau oligomer in human frontal cortices. **A:** AFM images of granular tau oligomers from representative Braak NFT-staged samples. Cases 1, 8, 14, and 18 were staged at Braak 0, I, III, and V, respectively. The size of each image size is 2 μm^2, and the height range is 30 nm. **B:** Quantitative data of granular tau oligomer is represented as the area (μm^2) occupied by tau granules. Each case and Braak NFT stage is indicated. **C,D:** Correlations between granular tau oligomer and tau levels (C) and oligomer and Hsp90 levels (D) are shown. Samples were grouped into Braak NFT stage 0 (squares) and Braak stages I, III, and V (diamonds).

fluorescent signals (data not shown). Because Hsp40 and Hsp70 form the initial recognition complex during the processing of client proteins of the chaperone network (Dickey et al., 2007), we added these HSPs to heparin-induced tau assembly preparations. Hsp40 and Hsp70 significantly reduced the ThT signals, but adding both Hsp40 and Hsp70 to the preparation reduced fluorescence even more, affecting tau assembly during the entire incubation period (Fig. 5). Interestingly, Hsp40 had a dose-dependent effect, whereas Hsp70 did not (Fig. 5B). These results indicate that Hsp40 and/or Hsp70 directly prevented the aggregation of tau protein. Further studies will be needed to clarify the refolding and degradation of tau protein related to molecular chaperones.

DISCUSSION

More than 20 neurodegenerative disorders are characterized by the presence of aggregates of the microtubule-binding protein tau (Lee et al., 2001). Tau protein forms insoluble NFTs that accompany and may promote neurodegeneration in these brain diseases. Details of the steps involved in the conversion of solu-

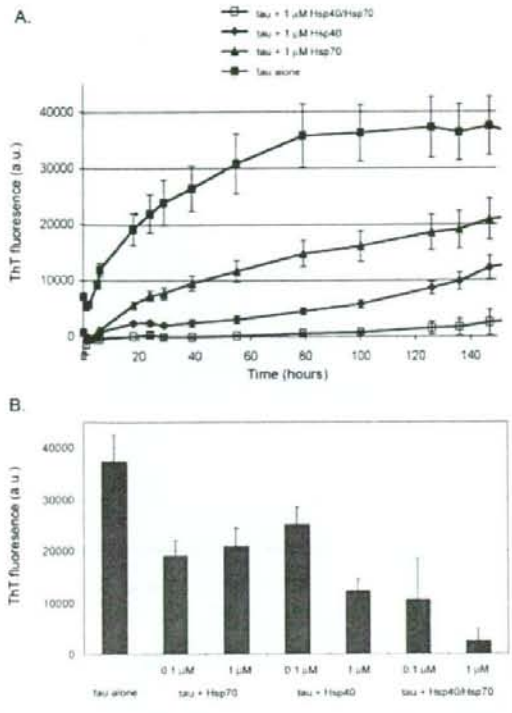

Fig. 5. Effects of Hsp40 and/or Hsp70 on in vitro tau self-assembly (solid squares). **A:** Heparin-induced tau aggregation was assessed by measuring ThT fluorescence at the indicated time points (mean ± SD; n = 5). Hsp40 (diamonds), Hsp70 (triangles), and Hsp40 + Hsp70 (open squares) were added to the aggregation reaction mixture at time zero. **B:** Tau aggregation levels are shown as a function of ThT fluorescence intensity (mean ± SD; n = 5). Tau was incubated with heparin in the presence of Hsp40, Hsp70, or Hsp40 + Hsp70 at the indicated concentrations for 147 hr.

ble tau to insoluble tau having a β-sheet conformation remain unclear. Recent studies have suggested the involvement of multiple degradation pathways in this process that require the action of molecular chaperones (Dou et al., 2003; Petrucelli et al., 2004). Here, we found that molecular chaperone-mediated tau protein metabolism plays a possible role in converting soluble tau to granular tau oligomer (intermediates of tau filaments) in human brain. Indeed, the levels of TBS-soluble tau correlated well with those of Hsp90, Hsp40, Hsp27, α-crystallin, and CHIP. In contrast to the levels of TBS-soluble tau, the levels of granular tau oligomer were inversely proportional to those of HSPs. In addition, our in vitro study showed that Hsp40 and Hsp70 proteins prevented tau aggregation. Taken together, these findings indicate that a molecular chaperone-tau protein processing pathway likely controls the initial phase of tau aggregation.

Together with comparative biochemical analyses of tau aggregates, electrophoretic profiles of pathological tau protein have allowed the molecular classification of tauopathies. Indeed, tauopathies differ in both tau phosphorylation and tau isoform content (Lee et al., 2001; Sergeant et al., 2005). Although electrophoretic tau protein profiles in various tauopathies have been well characterized, variations in tau protein levels have not been examined extensively, because studies of autopsy samples can be complicated by variability in disease severity, agonal state, age, environmental factors, and post-mortem delays. In the present study, we observed that TBS-soluble tau levels varied across different Braak stages, whereas β-actin, GAPDH, and NSE levels remained steady across different Braak stages. Moreover, the levels of TBS-soluble tau correlated well with those of Hsp90, Hsp40, Hsp27, α-crystallin, and CHIP. These variations were not related to post-mortem interval times, so it was unlikely that these protein levels were affected by post-mortem interval. In addition to chaperone protein levels, Akt and β-tubulin levels also positively correlated with TBS-soluble tau levels. Akt is known to be an Hsp90 client protein (Basso et al., 2002), and β-tubulin is known to be a component of microtubules that are stabilized by tau protein. Therefore, Akt, β-tubulin, and tau protein levels may also be regulated by the chaperone complex through a similar processing pathway.

Recently, our group described the quantitative analysis of a granular-shaped prefilamentous form of tau, the granular tau oligomer, in human brain (Maeda et al., 2006, 2007). We observed increased levels of granular tau oligomer in the frontal cortices staged at Braak I, suggesting that tau dysfunction had already occurred in frontal cortex by the time NFTs formed in entorhinal cortex. In the present study, we observed an inverse correlation between granular tau oligomer and HSP levels, the latter of which positively correlated with soluble tau protein levels. This inverse correlation was more significant when Braak 0 samples were excluded from our analysis. Braak NFT staging traces the gradual development of neurofibrillary changes in brain (Braak and Braak, 1991; Braak et al., 1994). Stage I is characterized by neurodegeneration of specific projection cells in the transentorhinal region, whereas Braak 0 is characterized by the absence of NFTs. Although we did not detect NFTs in the frontal cortices of Braak 0 and Braak I brains, the levels of granular tau oligomer and Hsp27 in Braak I samples were elevated. Because Hsp27 preferentially interacts with a hyperphosphorylated tau variant in human samples (Shimura et al., 2004a), it is possible that hyperphosphorylated prefilamentous tau was already induced in the frontal cortices of Braak I brains. With regard to the inverse correlation between granular tau oligomer and HSP levels, reduction of stress response can explain the increase in granular tau oligomers after the start of neurofibrillary changes. Because aging is a risk factor for various neurodegenerative disorders,

including AD, and the aging process is associated with gradual accumulation of oxidative stress factors (Coyle and Puttfarcken, 1993), it seems reasonable that the overriding of oxidative insults disables molecular chaperones.

Dickey et al. (2006a) reported that HSP induction mediates proteasome-dependent tau degradation. They found that Hsp90 inhibitors reduced the levels of tau phosphorylated at proline-directed Ser/Thr sites (pS202/T205, pS396/S404) and conformationally altered (MC-1) tau species that are induced by Hsp70, Hsp40, and Hsp27. Although Dickey et al. used an in vitro experimental system comprising P301L mutated tau-expressing H4 and CHO cells (Dickey et al., 2006a), a system that is completely different from our in vivo experimental system involving the protein profiling of human brains, Dickey et al.'s data were consistent with our results showing an inverse correlation between HSPs and MC-1-immunoreactive granular tau oligomers (Maeda et al., 2007). Still, we do not know whether the activation of multiple chaperone systems or inactivation of Hsp90 is induced by stress responses that occur during brain aging. However, because Hsp90 client proteins, such as Akt, are also related to HSP levels in human brain, it is likely that the Hsp90 chaperoning cycle mediates tau protein metabolism. Results from coimmunoprecipitation and in vitro tau assembly assays demonstrated that physiological interactions occur between tau and Hsp70. Hsp70 is well known to be a prominent HSP in eukaryotic cytosol (Hartl and Hayer-Hartl, 2002). Hsp70 function not only is modulated by Hsp40 to initiate protein refolding but is also associated with CHIP to process the ubiquitin-proteasome pathway (Dickey et al., 2007). Therefore, it seems likely that Hsp70 is also involved in chaperone-mediated tau protein metabolism.

Tau protein has been reported to be a substrate for a number of proteases, such as trypsin, chymotrypsin, cathepsin D, calpains, caspases, proteasomal proteases, and thrombin. Decreased proteasome activity in AD brains has been previously reported (Keller et al., 2000; Lopez Salon et al., 2000; Keck et al., 2003). The inhibition of Hsp90-mediated tau clearance by a proteasomal inhibitor has been also reported (Dickey et al., 2006a). The lysosomal pathway may represent a secondary pathway for HSP-mediated tau degradation. An alternative tau degradation pathway is chaperone-mediated autophagy (CMA). Recently, α-synuclein has been shown to be a substrate for CMA (Cuervo, 2004) and to be modulated by cochaperone CHIP for degradation via CMA (Shin et al., 2005). Our findings strongly suggest that molecular chaperone-mediated tau protein metabolism is a major regulator of the formation of abnormal oligomeric complexes of tau. Therefore, molecular chaperones might be promising targets in the development of therapeutics for diseases characterized by neurofibrillary degeneration as well as for other diseases characterized by protein conformational disorders. Further studies are necessary to determine the precise status of tau protein as a molecular chaperone client.

ACKNOWLEDGMENTS

We are grateful to Dr. Peter Davies (Albert Einstein College of Medicine) for providing us with PHF-1 antibody and to Dr. Ryosuke Takahashi (Graduate School of Medicine, Kyoto University) for providing us with CHIP antibody.

REFERENCES

Alonso AC, Grundke-Iqbal I, Iqbal K. 1996. Alzheimer's disease hyperphosphorylated tau sequesters normal tau into tangles of filaments and disassembles microtubules. Nat Med 2:783–787.

Arriagada PV, Growdon JH, Hedley-Whyte ET, Hyman BT. 1992. Neurofibrillary tangles but not senile plaques parallel duration and severity of Alzheimer's disease. Neurology 42:631–639.

Basso AD, Solit DB, Chiosis G, Giri B, Tsichlis P, Rosen N. 2002. Akt forms an intracellular complex with heat shock protein 90 (Hsp90) and Cdc37 and is destabilized by inhibitors of Hsp90 function. J Biol Chem 277:39858–39866.

Braak E, Braak H, Mandelkow EM. 1994. A sequence of cytoskeleton changes related to the formation of neurofibrillary tangles and neuropil threads. Acta Neuropathol 87:554–567.

Braak H, Braak E. 1991. Neuropathological stageing of Alzheimer-related changes. Acta Neuropathol 82:239–259.

Coyle JT, Puttfarcken P. 1993. Oxidative stress, glutamate, and neurodegenerative disorders. Science 262:689–695.

Cuervo AM. 2004. Autophagy: in sickness and in health. Trends Cell Biol 14:70–77.

Dabir DV, Trojanowski JQ, Richter-Landsberg C, Lee VM, Forman MS. 2004. Expression of the small heat-shock protein alphaB-crystallin in tauopathies with glial pathology. Am J Pathol 164:155–166.

Dickey CA, Dunmore J, Lu B, Wang JW, Lee WC, Kamal A, Burrows F, Eckman C, Hutton M, Petrucelli L. 2006a. HSP induction mediates selective clearance of tau phosphorylated at proline-directed Ser/Thr sites but not KXGS (MARK) sites. FASEB J 20:753–755.

Dickey CA, Yue M, Lin WL, Dickson DW, Dunmore JH, Lee WC, Zehr C, West G, Cao S, Clark AM, Caldwell GA, Caldwell KA, Eckman C, Patterson C, Hutton M, Petrucelli L. 2006b. Deletion of the ubiquitin ligase CHIP leads to the accumulation, but not the aggregation, of both endogenous phospho- and caspase-3-cleaved tau species. J Neurosci 26:6985–6996.

Dickey CA, Kamal A, Lundgren K, Klosak N, Bailey RM, Dunmore J, Ash P, Shoraka S, Zlatkovic J, Eckman CB, Patterson C, Dickson DW, Nahman NS Jr, Hutton M, Burrows F, Petrucelli L. 2007. The high-affinity HSP90-CHIP complex recognizes and selectively degrades phosphorylated tau client proteins. J Clin Invest 117:648–658.

Dou F, Netzer WJ, Tanemura K, Li F, Hartl FU, Takashima A, Gouras GK, Greengard P, Xu H. 2003. Chaperones increase association of tau protein with microtubules. Proc Natl Acad Sci U S A 100:721–726.

Gamblin TC, Chen F, Zambrano A, Abraha A, Lagalwar S, Guillozet AL, Lu M, Fu Y, Garcia-Sierra F, LaPointe N, Miller R, Berry RW, Binder LI, Cryns VL. 2003. Caspase cleavage of tau: linking amyloid and neurofibrillary tangles in Alzheimer's disease. Proc Natl Acad Sci U S A 100:10032–10037.

Garcia-Sierra F, Ghoshal N, Quinn B, Berry RW, Binder LI. 2003. Conformational changes and truncation of tau protein during tangle evolution in Alzheimer's disease. J Alzheimers Dis 5:65–77.

Hartl FU, Hayer-Hartl M. 2002. Molecular chaperones in the cytosol: from nascent chain to folded protein. Science 295:1852–1858.

Hasegawa M, Smith MJ, Goedert M. 1998. Tau proteins with FTDP-17 mutations have a reduced ability to promote microtubule assembly. FEBS Lett 437:207–210.

Hatakeyama S, Matsumoto M, Kamura T, Murayama M, Chui DH, Planel E, Takahashi R, Nakayama KI, Takashima A. 2004. U-box protein carboxyl terminus of Hsc70-interacting protein (CHIP) mediates polyubiquitylation preferentially on four-repeat Tau and is involved in neurodegeneration of tauopathy. J Neurochem 91:299–307.

Imai Y, Soda M, Hatakeyama S, Akagi T, Hashikawa T, Nakayama KI, Takahashi R. 2002. CHIP is associated with Parkin, a gene responsible for familial Parkinson's disease, and enhances its ubiquitin ligase activity. Mol Cell 10:55–67.

Jicha GA, Berenfeld B, Davies P. 1999. Sequence requirements for formation of conformational variants of tau similar to those found in Alzheimer's disease. J Neurosci Res 55:713–723.

Katsuno T, Morishima-Kawashima M, Saito Y, Yamanouchi H, Ishiura S, Murayama S, Ihara Y. 2005. Independent accumulations of tau and amyloid beta-protein in the human entorhinal cortex. Neurology 64:687–692.

Keck S, Nitsch R, Grune T, Ullrich O. 2003. Proteasome inhibition by paired helical filament-tau in brains of patients with Alzheimer's disease. J Neurochem 85:115–122.

Keller JN, Hanni KB, Markesbery WR. 2000. Impaired proteasome function in Alzheimer's disease. J Neurochem 75:436–439.

Kuret J, Chirita CN, Congdon EE, Kannanayakal T, Li G, Necula M, Yin H, Zhong Q. 2005. Pathways of tau fibrillization. Biochim Biophys Acta 1739:167–178.

Lee VM, Goedert M, Trojanowski JQ. 2001. Neurodegenerative tauopathies. Annu Rev Neurosci 24:1121–1159.

Lopez Salon M, Morelli L, Castano EM, Soto EF, Pasquini JM. 2000. Defective ubiquitination of cerebral proteins in Alzheimer's disease. J Neurosci Res 62:302–310.

Maeda S, Sahara N, Saito Y, Murayama S, Ikai A, Takashima A. 2006. Increased levels of granular tau oligomers: an early sign of brain aging and Alzheimer's disease. Neurosci Res 54:197–201.

Maeda S, Sahara N, Saito Y, Murayama M, Yoshiike Y, Kim H, Miyasaka T, Murayama S, Ikai A, Takashima A. 2007. Granular tau oligomers as intermediates of tau filaments. Biochemistry 46:3856–3861.

Muchowski PJ, Wacker JL. 2005. Modulation of neurodegeneration by molecular chaperones. Nat Rev 6:11–22.

Nemes Z, Devreese B, Steinert PM, Van Beeumen J, Fesus L. 2004. Cross-linking of ubiquitin, HSP27, parkin, and alpha-synuclein by gamma-glutamyl-epsilon-lysine bonds in Alzheimer's neurofibrillary tangles. FASEB J 18:1135–1137.

Petrucelli L, Dickson D, Kehoe K, Taylor J, Snyder H, Grover A, De Lucia M, McGowan E, Lewis J, Prihar G, Kim J, Dillmann WH, Browne SE, Hall A, Voellmy R, Tsuboi Y, Dawson TM, Wolozin B, Hardy J, Hutton M. 2004. CHIP and Hsp70 regulate tau ubiquitination, degradation and aggregation. Hum Mol Genet 13:703–714.

Sahara N, Murayama M, Mizoroki T, Urushitani M, Imai Y, Takahashi R, Murata S, Tanaka K, Takashima A. 2005. In vivo evidence of CHIP up-regulation attenuating tau aggregation. J Neurochem 94:1254–1263.

Saito Y, Nakahara K, Yamanouchi H, Murayama S. 2002. Severe involvement of ambient gyrus in dementia with grains. J Neuropathol Exp Neurol 61:789–796.

Sato S, Tatebayashi Y, Akagi T, Chui DH, Murayama M, Miyasaka T, Planel E, Tanemura K, Sun X, Hashikawa T, Yoshioka K, Ishiguro K, Takashima A. 2002. Aberrant tau phosphorylation by glycogen synthase kinase-3beta and JNK3 induces oligomeric tau fibrils in COS-7 cells. J Biol Chem 277:42060–42065.

Schweers O, Mandelkow EM, Biernat J, Mandelkow E. 1995. Oxidation of cysteine-322 in the repeat domain of microtubule-associated protein tau controls the in vitro assembly of paired helical filaments. Proc Natl Acad Sci U S A 92:8463–8467.

Sergeant N, Delacourte A, Buee L. 2005. Tau protein as a differential biomarker of tauopathies. Biochim Biophys Acta 1739:179–197.

Sherman MY, Goldberg AL. 2001. Cellular defenses against unfolded proteins: a cell biologist thinks about neurodegenerative diseases. Neuron 29:15–32.

Shimura H, Miura-Shimura Y, Kosik KS. 2004a. Binding of tau to heat shock protein 27 leads to decreased concentration of hyperphosphorylated tau and enhanced cell survival. J Biol Chem 279:17957–17962.

Shimura H, Schwartz D, Gygi SP, Kosik KS. 2004b. CHIP-Hsc70 complex ubiquitinates phosphorylated tau and enhances cell survival. J Biol Chem 279:4869–4876.

Shin Y, Klucken J, Patterson C, Hyman BT, McLean PJ. 2005. The cochaperone carboxyl terminus of Hsp70-interacting protein (CHIP) mediates alpha-synuclein degradation decisions between proteasomal and lysosomal pathways. J Biol Chem 280:23727–23734.

Takashima A, Murayama M, Murayama O, Kohno T, Honda T, Yasutake K, Nihonmatsu N, Mercken M, Yamaguchi H, Sugihara S, Wolozin B. 1998. Presenilin 1 associates with glycogen synthase kinase-3beta and its substrate tau. Proc Natl Acad Sci U S A 95:9637–9641.

Asymptomatic Self-Limiting Diffuse White Matter Lesions in Subacute to Chronic Stage of Herpes Simplex Encephalitis

A.M. TOKUMARU, K. KAMAKURA, H. TERADA, O. KOBAYASHI, A. KANEMARU, T. KATO, S. MURAYAM, M. YAMAKAWA, M. MIZUNO

Department of Radiology, Tokyo Metropolitan Medical Center of Gerontology; Tokyo, Japan

Key words: herpes simplex encephalitis, MRI, white matter, immune-mediated

SUMMARY – *This study evaluated white matter changes in the subacute and chronic stages of herpes simplex encephalitis (HSE). Subjects comprised 15 patients with HSE. All patients were examined using MRI at onset, and then at seven to ten days, three to five weeks and two to three months after onset. In addition, the six patients who displayed white matter signal abnormalities were examined at six months and >one year after onset. Cell count, protein levels, polymerase chain reaction (PCR) of herpes simplex virus in cerebrospinal fluid (CSF), and exacerbation of neurological symptoms as well as dose of acyclovir were compared between patients with and without white matter abnormalities. Diffuse white matter signal changes were identified at the subacute stage (3-5 weeks after onset) of HSE in six patients (6/15, 40%). No significant relationship was observed between the presence of white matter signal abnormalities and laboratory data, acyclovir dose or clinical symptoms. These signal abnormalities disappeared or improved by two years without any clinical treatment. Diffuse white matter signal abnormalities occur frequently in the subacute stage of HSE. Although the mechanisms underlying these white matter lesions have not been elucidated, subclinical immune-mediated processes may be considered. Repeat MRI studies over a long period are necessary for evaluating the clinical process of patients with HSE.*

Introduction

Herpes simplex encephalitis (HSE) is a life-threatening encephalitis caused by HSV-1 and HSV-2. Early recognition and prompt commencement of antiviral therapy significantly reduce mortality and morbidity. Although many patients experience severe after-effects, even with early acyclovir therapy, most MRI studies have investigated HSE in the acute stages, and few long-term follow-up studies have been reported. A small number of studies have revealed delayed white matter changes in the subacute and chronic stages [1-4].

The purpose of this study was to investigate how many white matter signal abnormalities are produced in patients with HSE using repeated follow-up MRI. Relationships between white matter abnormalities and other factors, including exacerbation of neurological findings, protein levels, cell counts in cerebrospinal fluid (CSF), polymerase chain reaction (PCR) in CSF and dose of acyclovir, were evaluated.

Patients and Methods

Repeated follow-up MRI was performed in 15 consecutive patients (10 men, 5 women) with HSE diagnosed using PCR methods. Mean patient age was 38 years (range, 10-54 years). MRI was performed in the acute stage, at seven to ten days, at three to five weeks, and at two to three months after onset. MRI was also performed at six months and at >one year after onset in six out of 15 patients who displayed white matter signal abnormalities. This study defined periods from onset to day ten as

acute stage, from third to fifth weeks as subacute stage, and two months later from onset as chronic stage.

All MR examinations were performed using a 1.5-T system. Fast spin-echo sequences were used for T2-weighted images (TR/TE=3500 ms/120 ms), T1-weighted images (TR/TE=500 ms/15 ms) and FLAIR images (TR/TE=10000 ms/120 ms), and diffusion-weighted images (spin-echo EPI: TR/TE=5000 ms/139 ms; b=1000 s/mm^2) were added in one of 15 cases.

All images were reviewed by two neuroradiologists blinded to patient information. Neurological findings were examined by neurologists or a pediatric neurologist. Mann-Whitney-U test was used for analyses. Cell count, protein levels and PCR of HSV in CSF and exacerbation of neurological findings, as well as dose of acyclovir, were statistically compared between patients with and without white matter abnormalities.

Patient details, including age, sex, period and dosage of drugs used for therapy, and white matter abnormalities are shown in table 1.

Results

Diffuse hyperintensity in the white matter was seen in six of the 15 patients (40%). These six patients presented widespread white matter lesions in the subacute to chronic phase. Although no white matter signal changes were identified on MRI between one week after onset and the tenth day, white matter signal changes were identified in five cases during the follow-up performed three weeks later, and in one case, unable to undergo follow-up three weeks later, in the examination performed five weeks later. After two months, the reduction process of the white matter signal changes was confirmed in only one pediatric case, but no obvious reduction tendencies were observed in the signal changes in the other five cases. In the follow-up at six months, although the white matter signal changes were prolonged in all six cases, reduction tendencies were identified, while in the search performed between the 14th month and two years after onset, reduction tendencies of the white matter signal changes, as well as local atrophy, were confirmed in all cases. All six cases showing white matter signal changes, cortical lesions, with bloating and hyperintensity on T2-weighted images in the acute stage, already manifested atrophic change. In addition, there were obvious features such as necrosis and bleeding in some areas. Distribution of white matter lesions is more widespread than that of gray matter lesions in the acute phase. *Case* 1 presented diffuse white matter hyperintensity on T2-weighted images in the left temporal and deep temporal lobe adjacent to affected gray matter lesions at three weeks after onset. Signal changes were also shown in the ipsilateral extreme capsules and claustrum (figure 1). Five of six cases had more widespread distribution of white matter lesions than gray matter lesions in the acute phase (figure 2).

Despite the apparent worsening of MRI findings, all patients remained neurologically stable. Clinical relapse was not shown in any patient. No significant statistical relationships were identified between the presence of white matter hyperintensities and cell count and protein levels, PCR of HSE in CSF, neurological findings or dose of acyclovir.

Discussion

Most previous studies on HSE have focused on MRI findings in the acute phase, but some case reports have described delayed white matter changes in the subacute or chronic stages [1-3]. The present study frequently detected (40%) asymptomatic white matter lesions in the subacute to chronic stages of HSE. White matter signal abnormalities occurring during the course of HSE have rarely been reported to date, but the present report shows that these changes are relatively common.

According to our cases and those reported by Ueda and Mitsufuji et Al [1,2], clinical and neurological exacerbation was not seen when white matter signal abnormality occurred, and thus it was difficult to regard such an event as a clinical relapse. There was no exacerbation of PCR in CSF, protein or cell count, which are acute stage indicators for HSE. However, each new white matter signal change in HSE showed atrophic change at the chronic stage, although it was self-limiting. Therefore, it is necessary to analyze pathogenesis in the future, including the possibility of these cases showing subclinical relapse.

According to a recent report by Sköldenberg et Al, in HSE relapse, PCR negativity, a lack of acute CSF signs and a lack of neural and glial cells destruction were not necessarily regarded as indicators [4]. Of 22 analyzed cases, four showed relapse, showing rises in the levels of CD8 and IFN-γ in CSF, which were considered

Table1 Symptoms treatment and distribution of the white matter lesions associated with HSE in subacute to chronic stages *GM*: gray matter, *WM*: white matter, *T*: temporal lobe, *dT*: deep temporal lobe including hippocampus, *F*: fronral lobe. Definition of clinical relapse: A relapse was considered to have occurred if there were acute, suddenly appearing, new or aggravated symptoms and sings of focal encephalopathy with or without fever and without neurological symptoms secondary to severe pneumonia, septicaemia, metabolic disorder or other disease. Transient seizures, not giving rise to sequelae and occurring without concomitant symptoms, were not considered to constitute a relapse.

Case No	*Sex, age (years)*	*Symptoms at acute stage*	*Initial treatment*		*Affected site in acute phase*		*Affected site at 3 to 5 weeks*		*Subsidence of WM lesions*	*clinical relapse*	*Cell Count in CSF Cells/ 3 mm³ At 3W*	*Protein In CSF Mg/dl At 3W*
			IV Acyclovir	*corticosteroids*	*GM*	*WM*	*GM*	*WM*				
1	M54	Fever, decreased consciousness	Acyclovir 30mg/kg/day During 21days	0	Lt T, dT	–	Atrophy in lt T, dT	Lt T	+	–	10	58
2	F10	Fever, confusion	Acyclovir 30mg/kg/day During 14days	Dex 10 mg 7 days	Rt T, dT	–	Atrophy in rt T, dT	Bil T Rt F	+	–	18	43
3	M48	Fever, decreased consciousness	Acyclovir 30mg/kg/day During 14days	0	Bil T, dT	–	Atrophy in bil T, dT	Bil T Bil F	+	–	15	51
4	M36	Fever , vomiting, confusion, seizures	Acyclovir 30mg/kg/day During 21days	0	Lt T,dT	–	Atrophy in lt T,dT	Bil T Lt F	+	–	6	54
5	F48	Fever, decreased consciousness	Acyclovir 30mg/kg/day During 14 days	0	Rt T, dT	–	Atrophy in rt T, dT	Bil T Rt F	+	–	10	41
6	M27	Fever, confusion, severe headache	Acyclovir 30mg/kg/day During 14 days	Dex 16 mg 3 days	Bil T, dT	–	Atrophy in Bil T, dT	Bil T Bil F	+	–	12	43
7	M30	Fever, seizures, decreased consciousness	Acyclovir 30mg/kg/day During 14 days	Dex 16 mg 7 days	Lt T,dT	+ Transient Callosal lesion	Atrophy in lt T,dT	–		–	20	59
8	M19	Headache, fever, Confusions, vomiting	Acyclovir 30mg/kgday During 14 days	Dex 10 mg 7 days	Bil T, dT	–	Atrophy in Bil T, dT	–		–	14	54
9	F43	Fever, seizures confusions	Acyclovir 25mg/kg/day During 14 days	0	Lt T,dT	–	Atrophy in lt T,dT	–		–	8	56
10	F27	Fever,decreased consciousness	Acyclovir 30mg/kg/day During 21 days	0	Rt T, dT	–	Atrophy in rt T, dT	–		–	10	41
11	F46	Fever, confusions, Sever headache	Acyclovir 30mg/kg/day During 14 days	Dex 16 mg 5 days	Bil T, dT	–	Atrophy in Bil T, dT	–		–	20	48
12	M50	Headache, fever, Confusions, vomiting	Vidarabine 15mg/kg/day During 21 days	0	Rt T, dT	–	Atrophy in rt T, dT	–		–	12	39
13	M49	Fever,decreased consciousness	Acyclovir 30mg/kg/day During 21 days	0	Bil T, dT	–	Atrophy in Bil T, dT	–		–	18	50
14	M43	Fever, confusions, Sever headache	Acyclovir 30mg/kg/day During 14 days	0	Bil T, dT	–	Atrophy in Bil T, dT	–		–	15	44
15	M40	Fever, confusions Severe headache Transient seizures	Acyclovir 30mg/kg/day During 14 days	Dex 10 mg 7 days	Rt T, dT	–	Atrophy in rt T, dT	–		–	22	43

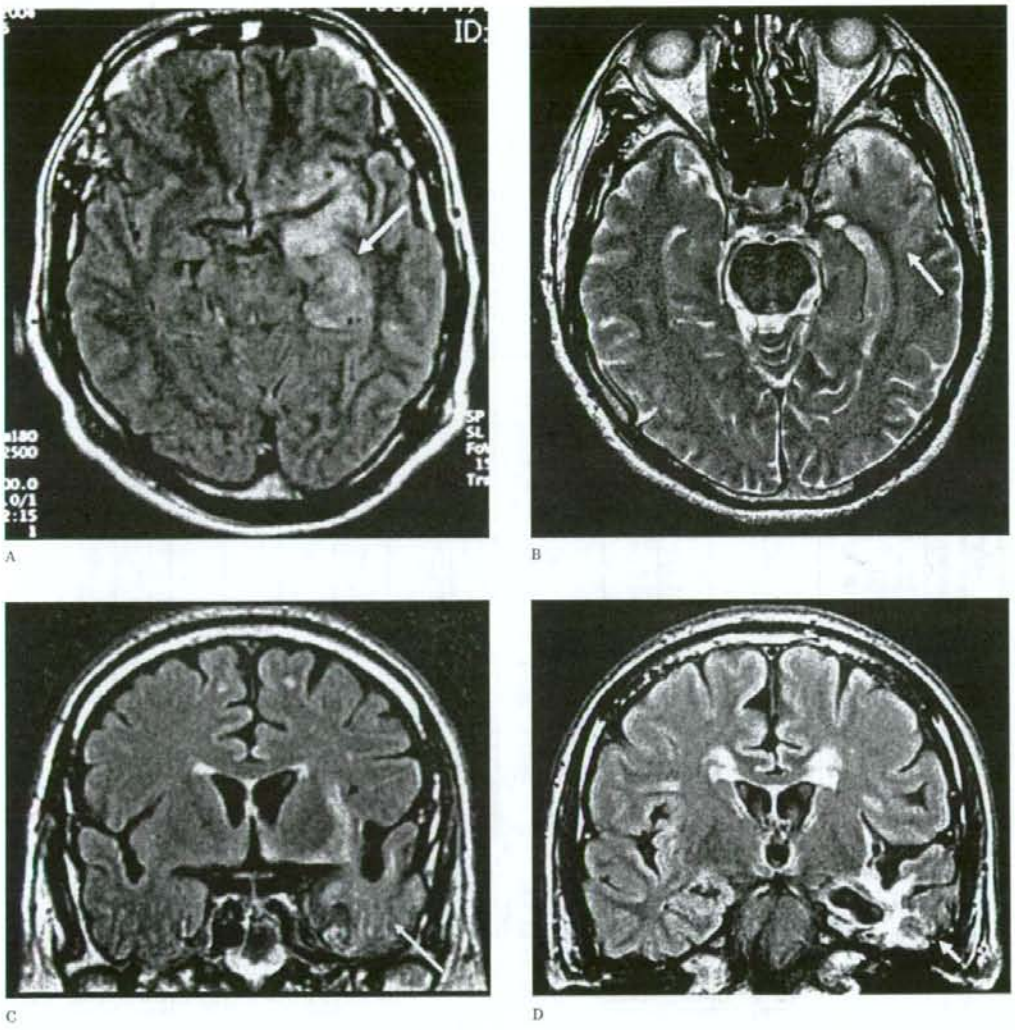

Figure 1 A-D A 54-year-old-male with HSE. A) FLAIR image at 2 days after onset shows hyperintensity with swelling in the left medial temporal cortices (white arrow). B) T2 weighted image at 3 weeks after onset shows hyperintensity in the left anterior temporal white matter (white arrow) and cortices. C) FLAIR coronal image at 3 weeks after onset demonstrates hyperintensity in the left temporal white matter (white arrow), left extreme capsule and claustrum (black arrowhead). D) FLAIR coronal image at 22 months after onset demonstrates that hyperintensiy in the left temporal white matter decreased in size with white matter volume loss. The medial temporal cortex showed severe damage with atrophy.

to indicate that immune activation is involved in the pathogenesis of HSE relapse. They suggested that these CSF findings, which indicate immunologically mediated pathogenesis, served as surrogate markers for HSE relapse. Unfortunately, in our analysis, CSF markers such as CD8 and IFN-γ were not examined, but we had sufficient follow-up imaging studies which were absent in their study; No obvious CT abnormalities were observed. MRI was performed

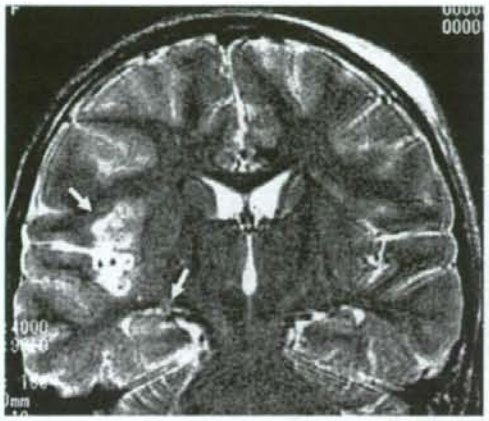

A

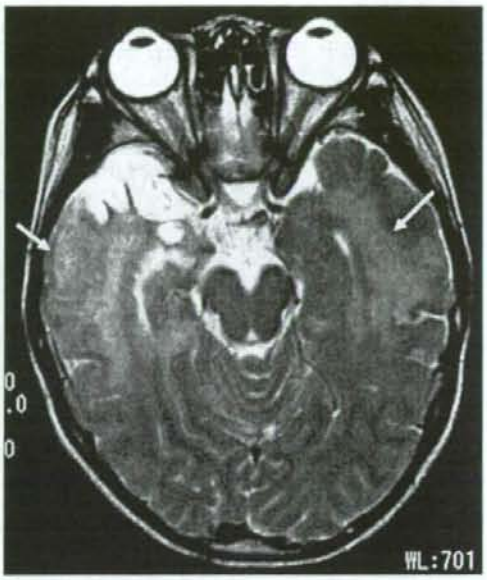

B

C

Figure 2 A-C A 10-year-old female with HSE. A) 3 days after onset. T2 weighted coronal image showed hyperintensity in the right hippocampus, parahippocampal gyri, right insula with swelling. Left parietal region of the scalp shows subcutaneous swelling and hyperintensity probably representing incidental hematoma. B) 3 weeks after onset. T2 weighted axial image shows hyperintensity in the bilateral temporal (white arrow) white matter. Right medial temporal cortices already show obvious atrophic change. C) 22 months after onset. Hyperintensity lesions in the bilateral temporal white matter improve.

in the fourth month after the start of symptoms in only one case, and there was a note saying "T2 gliosis oedema?" It would be interesting to see whether these findings corresponded to the white matter lesions we noted.

Persistence or recurrence (or reactivation) and/or immunologically mediated demyelinization of the brain tissue of HSV have been implicated in the pathogenesis of HSE relapse. The reason our cases showed a rise in white